Some expected impacts of a solar energetic particle event at Mars

F. Leblanc,[1] J. G. Luhmann,[2] R. E. Johnson,[3] and E. Chassefiere[1]

Received 27 August 2001; revised 22 November 2001; accepted 24 November 2001; published 24 May 2002.

[1] The effect of a typical solar energetic particle event on the Martian atmosphere is described. Sputtering, Lyman α emission, atmospheric heating, and the radiation flux at the surface are calculated using a model of the solar wind interaction with the Martian atmosphere. The effect of the crustal magnetic field is also investigated. We provide estimates of the associated escape flux of neutral atoms and molecules. We compare the atmospheric energy deposition due to the incident solar energetic particles with the energy deposition due to other sources such as solar EUV/IR, solar wind protons and Martian energetic neutral atoms derived from pickup ions. We show that atmospheric sputtering efficiency is small compared with that for pickup ions for the present epoch but that the energy deposition at the homopause is important compared with the EUV/IR energy deposition. While some areas of the atmosphere are shielded from the incident flux by the crustal magnetic fields, the energetic particle flux reaching the surface is virtually unattenuated. This study of "space weather" at Mars raises a number of questions that need to be addressed with new observations and models. *INDEX TERMS:* 1739 History of Geophysics: Solar/planetary relationships; 2459 Ionosphere: Planetary ionospheres (5435, 5729, 6026, 6027, 6028); 2780 Magnetospheric Physics: Solar wind interactions with unmagnetized bodies; 6225 Planetology: Solar System Objects: Mars; *KEYWORDS:* space weather, Mars, sputtering, heating, atmosphere

1. Introduction

[2] Three types of energetic particle events currently observed on Earth have been identified: gradual proton events (GPE), impulsive flare events, and corotating interaction region events [*Reames*, 1999]. The impulsive and gradual events are the most likely to affect a planetary atmosphere because they have the highest fluxes and frequency of occurence. Gradual proton and impulsive flare events are associated with populations of energetic ions from solar wind energy (1 keV/amu) to several hundred MeV/amu. They can have fluxes of 10^5, 10^3, 10^1, and 10^1 particles/(cm^2/s) of 1 MeV H, He, C, and O, respectively, at Earth orbit [*Reames et al.*, 1997a] and are highly dependent on solar activity. Such fluxes reaching Mars are of special interest because the Martian atmosphere and surface are poorly protected by the weak magnetic field and thin atmosphere. The purpose of this paper is to describe the effects initiated by the interaction of a solar energetic particle (SEP) event with Mars.

[3] Impulsive flare events are associated with solar eruptive flares, whereas a GPE is associated with the propagation of a coronal mass ejection (CME) in the interplanetary medium. The impulsive flare events are more frequent than the GPEs; roughly 100 impulsive flare events per year during solar maximum have been detected during the last 14 years, 50 times less during solar minimum, whereas only 10 GPEs per year have been observed during maximum solar activity [*Reames*, 1995; *Feynman et al.*, 1993]. However, impulsive flare events are associated, on average, with smaller fluxes, particularly at keV energies, are shorter in time (few hours for an impulsive flare events, whereas a GPE can last a few days), and have smaller dispersions in heliospheric longitude than GPE [*Reames*, 1999]. Here we focus on the encounter of a GPE with the Martian atmosphere because such events should have the strongest global effects on the atmosphere in terms of detectable heating, ionization, and atmospheric sputtering rates and should also have the highest intensity at the surface.

[4] When a GPE reaches Earth's magnetopause, the magnetospheric field may be compressed or eroded due to an accompanying interplanetary disturbance or CME, but it still protects the neutral atmosphere from direct interaction. Except at the locations of the strongest crustal fields [*Acuña et al.*, 2001; *Purucker et al.*, 2000], the principal obstacle to the interplanetary particles at Mars is the pileup of the solar magnetic field in the dayside magnetosheath and the bow shock. *McKenna-Lawlor et al.* [1998] reported a possible SEP event at Mars when Phobos 2 was operating. They reported a flux of particles crossing the Martian planetopause, the Mars counterpart of a magneto/ionopause solar wind boundary, without being significantly changed but also reported an increase of the flux of planetary escaping particles.

[5] Two stages are involved when describing the interaction and consequences of a SEP event. It is first important to determine which particle energies and fluxes reach Mars' exobase by determining how much the initial flux of SEP crosses the compressed magnetic field of the magnetosheath and the bow shock. As a first approximation, we will not consider the details of the encounter between Mars and the shock of the CME or its associated magnetic cloud [*Gosling and McComas*, 1987; *Burlaga*, 1991]. Indeed, a large fraction of the SEP reaches Mars before or after the CME itself passes through the magnetosheath. We will also consider the crustal magnetic field obstacle [*Purucker et al.*, 2000], which can lead to geographic irregularities in the flux reaching the exobase. We will not consider possible effects of the potential reconnection of the crustal magnetic field with the interplanetary magnetic field (IMF) [*Brain et al.*, 2001; *Luhmann et al.*, 2002]. Therefore induced and crustal fields will be treated independently, knowing that in any case the crustal magnetic field should have mainly local effects on the incident particle flux.

[1]Service d'Aéronomie du CNRS, Verrières-Le-Buisson, France.
[2]Space Science Laboratory, University of California, Berkeley, California, USA.
[3]Department of Engineering Physics, University of Virginia, Charlottesville, Virginia, USA.

0148-0227/02/2001JA900178$09.00

[6] After determining the flux at the exobase, we will describe the SEP effect on the Martian atmosphere. Before reaching the exobase, most of the incident solar ions are neutralized by charge exchange collision with the Mars exospheric hydrogen and oxygen [*Kallio and Luhmann*, 1997]. They then sputter the upper atmosphere, which consists mainly of O and CO_2. A direct consequence of this sputtering is to change the structure of the exosphere or Mars corona [*Johnson and Luhmann*, 1998; *Leblanc and Johnson*, 2001]. This, in turn, can affect the position of Mars' bow shock. However, modeling this feedback process is beyond the scope of this paper. Part of this new corona population will have enough energy to escape, while the bound part will provide a larger seed population for pickup ion production (picked up by the IMF frozen in the moving solar wind). Therefore an increase of both the escaping neutral and pickup ion flux should be expected from the SEP encounter. The SEP, with enough energy to penetrate into the atmosphere, can cause an amount of heating that depends locally on the dayside crustal field. In addition, the highest energy particles reach the surface.

[7] In section 2 we describe the method (section 2.1) used to calculate the flux reaching the exobase (section 2.2). In section 3 we investigate some of the effects produced: sputtering of the Martian atmosphere in section 3.1, Lyman α emission in section 3.2, atmospheric heating effects in section 3.3, local shielding due to the crustal magnetic field in section 3.4, and irradiation of the surface in section 3.5.

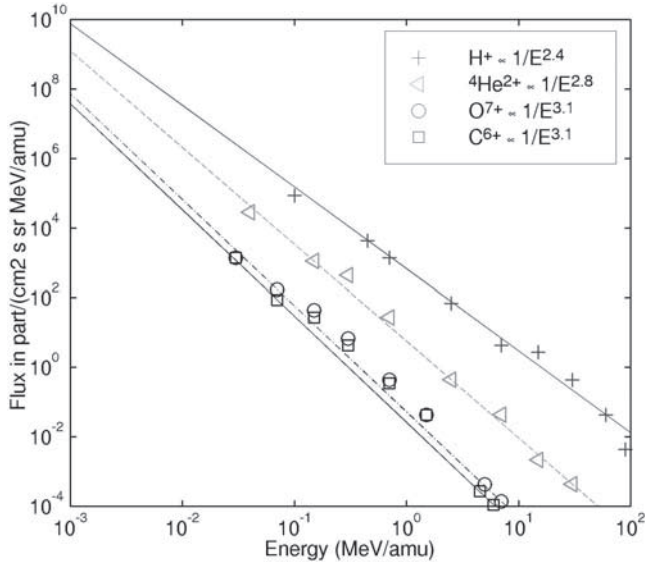

Figure 1. Gradual proton event of 20 October 1995 as reported by *Reames et al.* [1997a]. We here only reproduced the four main species and extrapolated the flux from Earth's orbit to Mars' orbit. We also make the fit with a power law up to solar wind energies. Values of the fit are indicated.

2. Shielding of the Martian Atmosphere

2.1. Model

2.1.1. Gradual proton event. [8] A GPE is first detected through its high, long duration (days) and flux of energetic particles but is also associated with a high-density plasma moving behind a large shock structure, which is supposed to be the main source of acceleration of the observed SEP [*Lee*, 1997; *Reames*, 1999]. This shock moves at an average speed of up to ~1000 km/s, but the associated SEP can be accelerated to much higher speeds and therefore are observed days before the arrival of the shock. A magnetic cloud with higher magnetic field intensity than the IMF is associated with the shock [*Gosling and McComas*, 1987; *Burlaga*, 1991]. A GPE is composed of many atomic species, but H, He, O, and C usually dominate [*Reames et al.*, 2001]. Figure 1 reproduces the GPE energy spectrum of 20 October 1995 reported by *Reames et al.* [1997a] for these four species. In Figure 1 we have extrapolated the profiles measured at Earth's orbit to Mars' orbit, assuming that such events expand roughly spherically in a heliocentric frame. These are typical flux spectra observed tens of hours before and after the shock in the 1–100 MeV/amu energy range [*Reames et al.*, 1997b] and close to the solar wind energy [*Baring et al.*, 1997]. Fe, Si, Ne, Mg, etc., are also observed in such an event. However, the net energy flux from these species is less important [*Reames et al.*, 1997a]. As will be shown, keV energy SEPs are particularly important in producing atmospheric effects.

[9] It is thought that keV energy particles in a GPE are directly accelerated from the solar wind [*Lee*, 1997; *Reames*, 1999], which is mainly H, He, O, and C [*Von Steiger et al.*, 2000]. The charge state of the ions for a GPE is roughly constant from 0.3 to 70 MeV and includes H^+, He^{2+}, C^{6+}, and O^{7+} [*Oetlicker et al.*, 1997]. The average solar wind charge states, H^+, He^{2+}, C^{6+}, and O^{6+} [*Von Steiger et al.*, 2000], are similar to those in a GPE.

[10] The flux energy spectra reported by *Reames et al.* [1997a] can be fitted to a power law [*Ellison and Ramaty*, 1985], as shown in Figure 1, down to the lowest energies. This fit is predicted by the theory of diffusive shock acceleration of particles [*Lee*, 1997]. It is in good agreement with the flux spectra observed at low energies from solar wind energies up to 10 MeV/amu both downstream and upstream from the shock [*Van Nes et al.*, 1984; *Ellison and Ramaty*, 1985]. It has been reported by *Gosling et al.* [1981] that such profiles are smoothly connected to the solar wind energy distribution at the shock, in good agreement with simulations of this acceleration process [*Jones and Ellison*, 1991; *Baring et al.*, 1997]. However, above 10 MeV/amu, this theory is not able to explain the observed profiles [*Lee*, 1997]. *Klein and Trottet* [2001] noted that both diffusive shock acceleration and preacceleration associated with flare eruption must operate to produce the observed high energy tail. The flux of SEP in Figure 1 will be used up to 100 MeV/amu. The flux is extrapolated down to 0.5, 1, 9, and 10 keV for H^+, He^{2+}, C^{6+}, and O^{7+}, respectively, as shown in Figure 2, where we assumed a solar wind velocity of 400 km/s and densities $n_H = 1$ cm^{-3}; $n_{He} = 0.05$ cm^{-3}; $n_O = 0.001$ cm^{-3}; and $n_C = 0.0007$ cm^{-3}, where n_H, n_He, n_O, and n_C are the density of H, He, O, and C, respectively. For each solar wind species we approximate its velocity distribution by a Maxwellian velocity distribution with temperatures equal to 10^5, 3×10^5, 12×10^5, and 9×10^5 K for H, He, O, and C, respectively [*Von Steiger et al.*, 1995]. Figure 2 shows that there is a good agreement between the flux of protons for the adopted SEP event and the solar wind but a higher relative flux in the SEP event for the other species. Following simulations and observations [*Baring et al.*, 1997; *Gosling et al.*, 1981], the shock-accelerated flux can be fit by a power law close to the injection energy (the solar wind energy) of the particles [*Jones and Ellison*, 1991]. Figure 2 proposes one possibility for this fit deduced from one particular set of observations [*Reames et al.*, 1997a]. Of course, the SEP flux is highly variable and can be, in some cases, a few orders more intense [*Mason et al.*, 1999]. Therefore this study is not comprehensive in its assumptions or results but is intended to identify and quantify atmospheric changes for one representative SEP event.

2.1.2. Mars' planetopause. [11] The Mars solar wind bow shock and the interplanetary magnetic field pileup in the magnetosheath are the two main obstacles that a solar particle has to cross before reaching the exobase. Both are derived from the interaction of the solar wind with Mars' ionosphere and remanent crustal fields. When a SEP event reaches Mars, the interplanetary conditions may change for up to several days to those characteristic of an interplanetary magnetic cloud [*Burlaga*, 1991]. Particles of energy >5keV/amu will encounter the bow shock and

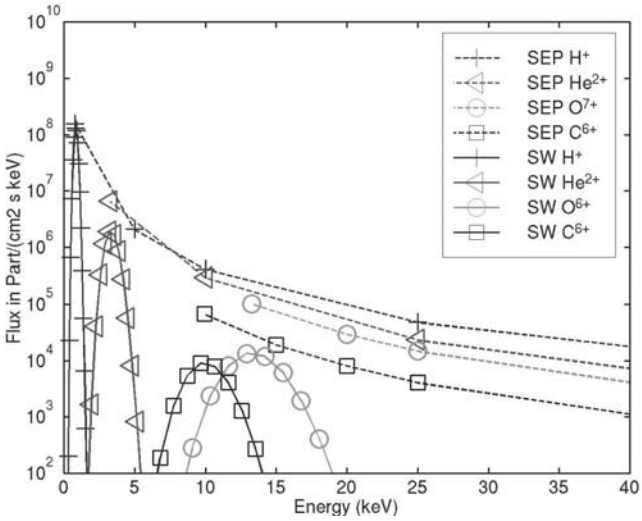

Figure 2. Same event as Figure 1 but zoomed at solar wind (SW) energy range. Also plotted in dashed lines is the solar wind flux H, He, C, and O for slow solar wind conditions. SEP, solar energetic particles.

magnetosheath ahead of the arriving shock. Below these energies the trajectories will not be accurately described using a model based only on the normal interaction of the solar wind with Mars. However, we will treat the whole range of energy with the same model for the bow shock and magnetic field pileup due to the interaction of the steady quiet solar wind with Mars. The magnetic cloud usually has a higher field magnitude than the IMF and often exhibits large north/south components. The higher ram pressure that occurs in the pileup solar wind preceding the cloud can push the Martian obstacle/solar wind boundary closer to the exobase. A mechanism that is not as important at Earth as at Mars is the increase of the mass loading, which can also significantly change the position of the bow shock [*Bauske et al.*, 1998; *Kallio et al.*, 1998].

[12] We use the combined crustal field and magnetosheath models described by *Luhmann et al.*, [2002]. The model of magnetic pileup and bow shock is based on a three-dimensional (3-D) MHD approach for typical quiet solar wind conditions, an average velocity of 400 km/s, a density of 1 proton per cm^3, and an IMF intensity of 4 nT with a Parker spiral angle of 90°. In such a case the IMF is perpendicular to the solar wind flow. Although the Parker spiral angle at Mars' orbit is equal to 56°, we used a 90° angle because this angle corresponds to a subsolar perpendicular shock for which incident particles are the most deflected before the exobase [*Brecht*, 1997b], giving a lower bound estimate of the flux penetrating Mars' exobase. The magnetic crustal field model used was derived by *Purucker et al.* [2000] from MGS magnetometer observations. For each magnetic field structure we follow thousands of ions representing the flux spectrum in Figure 1. Each particle is launched at several Mars radii from the surface on the dayside and with a velocity oriented along the Mars/Sun direction toward Mars. Each particle moves in the magnetic field as described by either the magnetosheath or crustal field model. We follow a particle until it is again at several radii from Mars or reaches an altitude 200 km. This is roughly the exobase altitude and also where much of the ion flux is neutralized by charge exchange [*Kallio and Luhmann*, 1997; *Zhang et al.*, 1993]. Figure 3 displays an example of H^+ and O^{7+} trajectories with solar wind energy and with energy 5 times larger moving around Mars in the combined magnetic field model. At such energies these particles have gyroradii of the same order as the Mars radius (the dark sphere Figure 3) with larger gyroradii for the O^{7+} than for the H^+. We count the particles reaching 200 km from the surface, the approximate exobase altitude, and note their energy and incident angle. A few hundreds of thousands are needed to then deduce the flux penetrating the atmosphere after averaging over the whole sphere at 200 km.

[13] Above 200 km, part of the ions is neutralized by charge exchange, mainly with neutral coronal H. This is true for particles with energy smaller than few keV/amu (for H^+ until 30 keV [e.g., *Johnson*, 1990]). Above such energy range the charge exchange cross section decays as $\sim v^{-12}$ with v the velocity of the impactor [*Johnson*, 1990]. Therefore high-energy particles remain charged deeper into the atmosphere. Below 200 km, neutral particles move mainly under the effect of collisions and of the gravity field. High-energy charged particles move also under the effect of the magnetic field. However, owing to their large gyroradius around the magnetic field lines (>1 R_m), their trajectory in the atmosphere from 200 km in altitude to Mars' surface is not significantly affected by the magnetic field. We will therefore describe all of the particles as moving only under the effect of the gravity field and atmospheric collisions below 200 km.

2.2. Flux at the Exobase

[14] The magnetic barrier effects on incident solar wind protons have been studied by *Brecht* [1997a, 1997b] and *Kallio and Koskinen* [1999] in the context of the IMF draping around an idealized Mars obstacle. These authors have shown that the

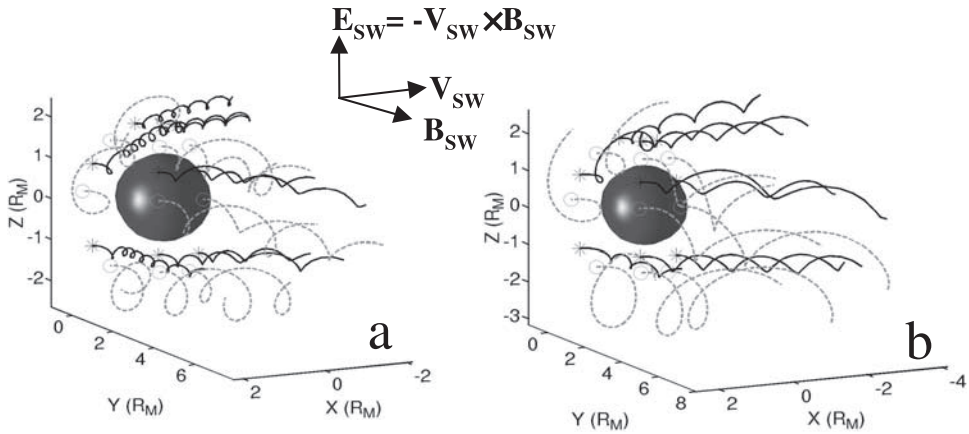

Figure 3. Trajectories of solar wind particles in the interplanetary magnetic field draped around Mars. (a) Solid lines show H^+ particles of 1 keV energy, and dashed lines show H^+ particles of 5 keV energy. (b) Solid lines show O^{7+} particles of 10 keV energy, and dashed lines show O^{7+} particles of 50 keV energy.

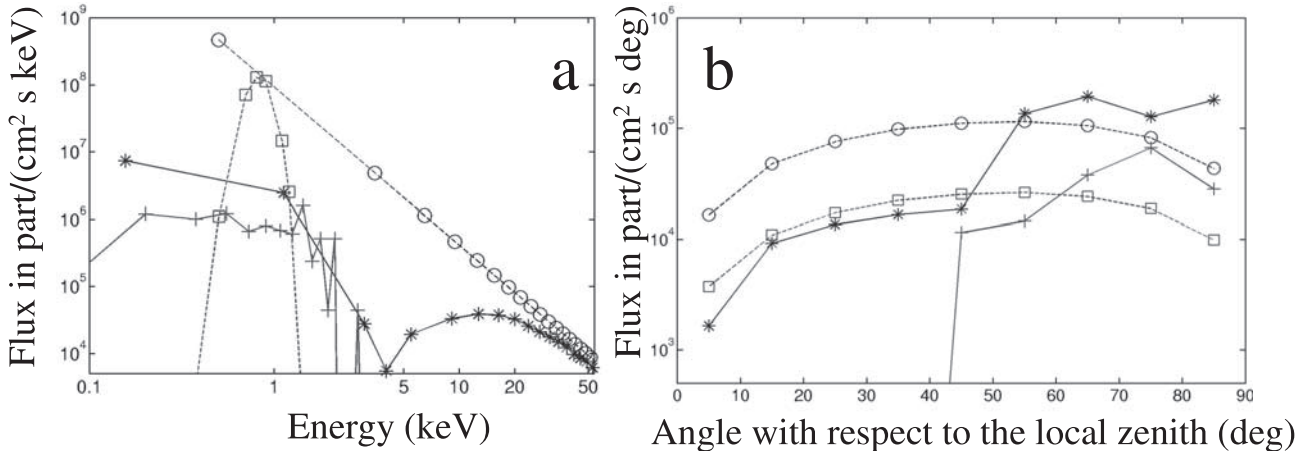

Figure 4. Flux of H^+ ions associated with the Gradual proton event reported in Figures 1 and 2. (a) Energy distribution. (b) Angle distribution. Circles show flux of solar energetic protons before the bow shock; stars show flux of solar energetic protons reaching the exobase; squares show flux of solar wind protons before the bow shock; and crosses show flux of solar wind protons reaching the exobase.

trajectories of these particles are altered by the magnetic field barrier and that only between 3 and 30% of solar wind protons reaches the exobase depending on the IMF/solar wind angle.

[15] It is the low-energy range of Figure 1 that is changed by crossing the magnetic field barrier, i.e., below 50, 80, 180, and 200 keV for the H^+, He^{2+}, C^{6+}, and O^{7+}, respectively. Above this energy a particle loses only a few percent of its initial energy between the interplanetary space and the exobase.

[16] Figures 4 and 5 present the flux at the exobase for H^+ and O^{7+}, respectively, in the range of energy where the initial flux is affected above the exobase. The fluxes of He^{2+} and C^{6+} at the exobase are roughly changed in the same way. In Figures 4 and 5 the circles represent the SEP fluxes as they are before the bow shock, and the stars represent the fluxes at the exobase. We also plotted in Figures 4 and 5 the change in the solar wind flux (squares) between the bow shock and the exobase. We found that only 1.7% of the solar wind and SEP protons, 6.0% of the solar wind and SEP He^{2+} and C^{6+} ions, 12% of the solar wind O^{6+}, and 9% of the SEP O^{7+} reach the exobase (percentage of solar particles that would have reached the exobase if no magnetic field was acting). This is roughly consistent with the 3% of solar wind protons that are captured by Mars for the same IMF orientation according to *Kallio and Luhmann* [1997] and *Brecht* [1997b]. It is also consistent with the property suggested by *Brecht* [1997b] that the capture efficiency is proportional to the square of the mass to charge ratio. The crosses line of Figure 4a can be compared to the dashed line corresponding to run 59 of *Brecht* [1997b, Figure 7a]. The flux profiles are similar with a peak around the solar wind energy and a slight energization above (due to finite gyroradius proton effect). Small differences arise, as Brecht used a solar wind velocity of 425 km/s and a solar wind density of 2 protons/cm^3. Our approach using solar wind test particles moving in the fields of a MHD model thus reproduces roughly the results of a self consistent hybrid model (see also the discussion on the accuracy of a similar approach by *Kallio and Barabash* [2001]).

[17] Figures 4a and 5a show that below the solar wind, energy particles are strongly deflected by the magnetic pileup and on average gain energy because of the finite gyroradius effect. Above this energy, particles are less deflected. This is due to the Lorentz force equal to $(\mathbf{V} - \mathbf{V}_{SW}) \times \mathbf{B}_{SW}$, where $\mathbf{V}$ is the velocity of the particle, $\mathbf{V}_{SW}$ the local velocity of the solar wind (SW) (along the $-x$ axis at $x > 2\ R_m$), and $\mathbf{B}_{SW}$ is the interplanetary magnetic field frozen in the solar wind (along the $+y$ axis at $x > 2\ R_m$). Particles after the bow shock that still have much larger velocity than the

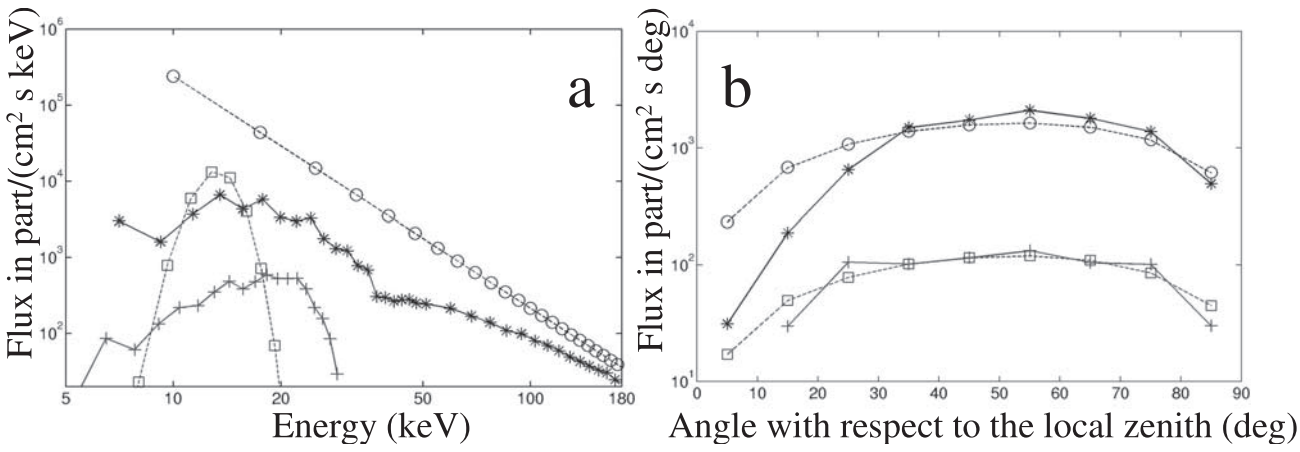

Figure 5. Flux of O^{7+} ions associated with the gradual proton event reported in Figure 1. (a) Energy distribution. (b) Angle distribution. Circle show flux of solar energetic O^{7+} before the bow shock; stars show flux of solar energetic O^{7+} reaching the exobase; squares show flux of solar wind O^{6+} before the bow shock; and crosses line shows flux of solar wind O^{6+} reaching the exobase.

solar wind velocity do not have their energy significantly changed by this force. On the contrary, particles that have velocity smaller than the solar wind velocity or of the order of the solar wind velocity are significantly affected by the Lorentz force. As a consequence, their kinetic energy is oscillating from zero to a value equal to several times the kinetic energy of a same mass particle with the velocity of the local solar wind. This explains the minimum in the flux of H and O (Figures 4a and 5a) around 4 and 40 keV, respectively. The flux at low energy at the exobase is partly due to particles of higher energies that lose energy before reaching the exobase. However, this contribution remains small since the initial flux of 5 keV H^+ is 2 orders of magnitude less than the flux of 1 keV H^+ (Figure 2).

[18] Figures 4b and 5b show the angular distribution of the incident particles penetrating the atmosphere: SEP (circles and stars) and solar wind (squares and crosses). The angle is measured between the particle velocity and the normal to the planet's surface so that 90° corresponds to a tangent trajectory to the surface, whereas 0° is normal downward. The initial profiles (circles and squares) are calculated for an uniform flux across a surface perpendicular to the Sun-Mars axis. Such a distribution projected onto the exobase displays a slight peak around 55°, which is similar to that used in the model of sputtering by pickup ions [*Luhmann et al.*, 1992]. This distribution is only roughly changed by the magnetic field barrier in the case of the O^{7+} ions (circles in Figure 5b) but is significantly changed for the H^+ ions (circles in Figure 4b). We also plot the angular distribution of the solar wind particles at the exobase (squares and crosses). More SEPs reach Mars' exobase with normal incidence because of their larger energy. The 0° angles are depleted because these particles arrive almost perpendicular to the atmosphere in the subsolar region where the magnetic pileup of the IMF generates the strongest barrier. The severe decrease of the flux of solar wind protons (crosses in Figure 4b) around the incident angle of 40° is related to the gyromotion of these particles, with gyroradius equal to $mV/(qB)$, where m and q are the mass and charge of the particle and B is the magnetic field strength. Indeed, the same severe decrease of the He^{2+} flux appears below 30° because the He^{2+} gyroradius is 2 times larger than the proton gyroradius. This decrease appears for the C^{6+} around 25°, as the C^{6+} gyroradius is slightly larger than the He^{2+} gyroradius. As shown in Figure 5b (crosses), this decrease takes place below 15° for the O^{7+} because these particles have a gyroradius 2.3 larger than the proton gyroradius. Overall, Figures 4b and 5b illustrate that low-energy particles are deflected and the highest energy particles are not. Therefore the latter penetrate the atmosphere with no significant change in their angular distribution.

[19] The results in Figures 4b and 5b are highly dependent on the Parker spiral angle of the IMF at Mars' orbit (chosen equal to 90° in this work) as well as the magnetosonic Mach number of the solar wind, which determines the magnetosheath thickness and magnetic field compression. For example, at low Mach numbers encountered during the passage of large magnetic clouds, the shock expands outward, and magnetosheath field draping and compression weaken [e.g., *Russell et al.*, 1993]. A radial IMF would produce almost no magnetic barrier at the nose of the magneto/ionopause and might introduce magnetosheath field fluctuations that scatter the ions [e.g., *Luhmann et al.*, 1983].

[20] The crustal fields can cause additional local effects as will be shown in section 3. However, when the impacting flux is averaged over the whole surface, the net effect of the crustal fields is small.

3. Atmospheric Changes

[21] In order to investigate the effects of the particles penetrating Mars' atmosphere, we track them through the neutral atmosphere below ~200 km. The results of our study lead to the following conclusions concerning the four species considered:

1. SEP hydrogen ions do not generate escape by atmospheric sputtering because of their relatively small mass compared with the principal constituents above 120 km: C, O, CO, and CO_2 [*Bougher and Roble*, 1991]. However, the energetic component of SEP protons generate the most heating and are the least affected by the atmosphere. Therefore most energetic SEP protons reach the surface.
2. SEP helium ions are also inefficient atmospheric sputtering agents because of their small mass but contribute to the total SEP heating of the atmosphere. The SEP helium ion flux at the surface is small compared with protons because of their smaller initial flux but also because the helium ions lose proportionally more energy through collisions in the atmosphere.
3. SEP oxygen ions do not reach the surface and deposit much less heat in the atmosphere (roughly 2 orders of magnitude less energy than the hydrogen ions) but efficiently sputter Mars' atmosphere and generate a significant escape flux.
4. SEP carbon ions have roughly the same impact on Mars' atmosphere as the oxygen ions but are slightly less efficient at sputtering Mars' atmosphere.

[22] In the following sections we describe atmospheric sputtering (section 3.1) by the oxygen and carbon ions, Lyman α emission (section 3.2) and heating (section 3.3) by hydrogen and helium and surface irradiation (section 3.5) by hydrogen. We also examine the effect of the crustal magnetic field in section 3.4. For the present study we neglect any effects of solar energetic electrons accelerated in flares or at the CME shock [e.g., *Lin*, 1985].

3.1. Atmospheric Sputtering

[23] In order to calculate atmospheric sputtering effects of the Martian atmosphere by SEPs, we use the spectra for the O (Figure 5) and C particles reaching the exobase with energy below 50 keV. Above 50 keV the atmospheric sputtering is not efficient since O and C atoms at such energies mainly lose energy by ionization.

[24] Since charge exchange transforms most of such incident ions to energetic neutrals by the time they reach the exobase [e.g., *Johnson et al.*, 2000], we simulate the effect of incident O and C atoms on Mars' atmosphere by using an 1-D Monte Carlo model. In this simulation we follow the impacting neutral particles moving in an atmosphere composed of C, O, CO_2, and CO. The model of Martian atmosphere is based on the works of *Zhang et al.* [1993] and *Bougher and Roble* [1991] and is the same model as the one used by *Leblanc and Johnson* [2002] for the present epoch. This method treats collisions between molecules or between molecules and atoms using a molecular dynamics approach. In this way we avoid the use of analytic models [*Johnson and Liu*, 1998] for collision cross sections, as by *Kass and Yung* [1995, 1996] (see also D. M. Kass and Y. L. Yung, Evolution of the Matian atmosphere: Results of a Monte Carlo model of sputtering, submitted to Icarus, 2001), since each collision is simulated separately by using the potentials of interaction [*Johnson and Liu*, 1998] between all of the atoms involved in the collision. As shown by *Leblanc and Johnson* [2002], this approach accurately describes incident energetic atoms penetrating a molecular atmosphere. For each species we follow ~10,000 incident particles representing the energy and angular distributions in Figure 5 for O. The number of collisions and the impact parameter are calculated following *Bird* [1994] algorithm. We follow all of the particles that have energy greater than the escape energy. The 3-D characteristics of the interaction of an incident flux with Mars' atmosphere has been described by *Leblanc and Johnson* [2001]. They conclude that the flux of escaping particles calculated with a 1-D approach should be increased by roughly 20% because of the grazing particles impacting Mars' atmosphere. Based on Figure 5b, this percentage is slightly higher since the proportion of grazing particles (incident angle of ~90°) inside the impacting population (solid star line) is increased by the deflection due to the IMF draping around Mars compared with the simpler flux (circle dashed line) used by *Leblanc and Johnson* [2001].

Table 1. Escaping Flux at the Exobase Due to O^{7+} and C^{6+} Incident Particles of the Gradual Proton Event Plotted in Figure 2 and Due to Pickup O^+ Ions [*Leblanc and Johnson*, 2002]

Incident/Escaping Species	O	CO_2	CO	C
SEP O^{7+}	5×10^{22}	3×10^{21}	3×10^{21}	1×10^{22}
SEP C^{6+}	1×10^{22}	1×10^{21}	1×10^{21}	4×10^{21}
Pickup O^+ ions	3×10^{23}	4×10^{22}	4×10^{21}	6×10^{22}

[25] The values of the escaping atmospheric neutral flux due to the sputtering by the impacting SEP are provided in Table 1. These have been calculated for the typical event described in Figure 1, extrapolated down to solar wind energy as shown in Figure 2, and partly deflected as shown in section 2.2. They correspond to 10^5 O atoms/(cm^2/s) affecting Mars' atmosphere and 5 10^4 C atoms/(cm^2/s). Except for CO, the escape fluxes in Table 1 are smaller than the ones generated by the pickup ions [*Luhmann and Kozyra*, 1991] for present solar minimum conditions [*Leblanc and Johnson*, 2002] with the flux of incident pickup ions $\sim 5\ 10^5 \times$ O atoms/(cm^2/s) at 1 keV [*Johnson and Luhmann*, 1998]. For such a flux, *Leblanc and Johnson* [2002] calculated escape fluxes, which are also provided in Table 1. The lower efficiencies are due to the larger average energy of the incident SEP. For instance, O^{7+} SEP is, on the average, 20% less efficient for ejecting atmospheric particles than a 1-keV pickup O^+. However, the net energy flux of the SEP is larger, producing more CO_2 dissociations and hence more ejected CO.

[26] The escape fluxes are also much smaller than that predicted by *Kim et al.* [1998] for dissociative recombination of the O_2^+ ions in Mars' atmosphere. However, impacting particles are the only known mechanism that can generate escaping neutral CO_2 and CO. Therefore a measurement of these two molecules in the vicinity of Mars will be useful to distinguish and calibrate the mechanisms for escape. The crustal magnetic field has only a small effect on the total escape flux because it only locally protects Mars' atmosphere (on the scale of few degrees in latitude and longitude), as shown in section 3.4.

3.2. Lyman α Emission

[27] *Kallio and Barabash* [2001] estimated the Lyman α emission due to $\sim 2 \times 10^{24}$ solar wind H atoms/s that are impacting the atmosphere and colliding with CO_2 atmospheric molecules. These authors calculated a peak emission of 100 Rayleighs and concluded that this is small compared with the kR emission of the dayside airglow. As shown here, the flux of energetic SEP protons at the exobase is $\sim 4 \times 10^{24}$ H/s. These have energies <10 keV and therefore efficiently neutralized before 200 km. However, the energy flux associated with these particles is an order of magnitude more than the energy flux calculated by *Kallio and Barabash* [2001]. Since the cross section for generating photon emission by H-CO_2 collision is roughly constant for impacting H atoms with energies from 500 to 10 keV [*Kallio and Barabash*, 2001], a SEP has roughly the same probability per collision of generating photon emission as a solar wind H. Therefore, because a H SEP is on average 5 times more energetic than a solar wind H particle, it generates ~5 times more Lyman α emission. Therefore the total Lyman α emission due to the incident solar energetic hydrogens has an intensity between 200 Rayleighs and 1 kR.

3.3. Heating

[28] In order to determine the heating due to a SEP event, we follow the O, C, H, and He SEPs penetrating Mars' atmosphere. For energies higher than 3 keV/amu the particles mainly lose energy and heat the atmosphere by ionization, so the Monte Carlo model described in the section 3.2, particularly developed to describe nuclear collision in a molecular atmosphere, is not needed. Therefore we use the stopping and range of ions in matter (SRIM) software [*Ziegler et al.*, 1985]. This 1-D software has been developed and adapted to describe the results of ions impacting gas and surfaces for a large range of energies and a large set of atomic species. It uses extrapolations of cross sections measured in the laboratory [*Eckstein*, 1991]. In order to investigate the energy deposition rate due to the impacting SEP, we consider a discrete energy distribution that has 14 ranges of energy from 1 keV/amu to 100 MeV/amu for each species. For each energy range we follow representative particles penetrating with normal incidence into the Martian atmosphere. We use an atomic Martian atmosphere model with equivalent atomic density, $N_O = 3\ n_{CO_2} + 2\ n_{CO} + n_O$, where n_{CO_2}, n_{CO}, and n_O are the densities in the Martian atmosphere of CO_2, CO, and O, respectively, used in section 3.1. Because the stopping effects of C and O are very similar but the relative amounts change with depth, for simplicity, we treat all of the atoms as O. Such an approximation for the Martian atmosphere has been shown to be roughly accurate for describing the total atomic escaping flux due to incident particles [*Leblanc and Johnson*, 2002]. We use SRIM results for the energy deposition rate versus depth given as a column of O and then convert that using the density profile into the energy deposition with altitude for each incident particle. We then compute the total amount of energy deposited by the incident flux from the exobase to the surface between 200–150, 150–130, and 130–110 km and from 110 to 0 km in layers 10 km thick. Using this method and the flux of penetrating protons into Mars' atmosphere for slow solar conditions as determined by *Kallio and Barabash* [2001], we can reproduce their results with roughly the same distribution with altitude and a peak around 120–130 km.

[29] Figure 6a compares the total energy deposition in eV/cm^3/s versus altitude (averaged over all the solar zenith angles) due to the flux of SEPs (triangles) with the EUV/UV energy deposition at a zenith angle of 45° (circles) from *Fox and Dalgarno* [1979]. We also plotted the energy deposition rate due to the incident energetic neutral atoms (ENA) as calculated by *Kallio and Barabash* [2001] for a zenith angle of 45° (squares line). We also give separately the solar energetic hydrogen (crosses) and helium (stars) components. The contribution of the impacting oxygen and carbon energetic particles is much smaller. Figure 6 shows that the encounter of a SEP event with Mars will generate peak heating between 105 and 120 km. This maximum is due to helium (stars) and hydrogen (crosses) with energies between 1 and 10 keV (which have been considered as neutralized before 200 km). The lower flux of helium compared to hydrogen in a SEP event (Figures 1 and 2) is compensated by the fact that helium more easily crosses Mars' bow shock and magnetic pileup.

[30] The EUV/UV efficiency for heating the atmosphere is roughly equal to 0.2 [*Fox and Dalgarno*, 1979; *Fox et al.*, 1995]. According to *Kallio and Barabash* [2001], only 14% of the energy deposited by the incident 800 eV solar wind H atoms is directly converted into neutral heating, mainly by collisions with CO_2 molecules. The other 86% is spent in inelastic processes, generating Lyman α emission (30%), ionization of the neutral atmospheric particles (27%), and electron stripping (ionization of the impacting particle) (26%). As a comparison, for 800 eV H, the SRIM software calculated that around 16% of the energy is deposited directly into neutral heating and 84% into electronic excitation, in very good

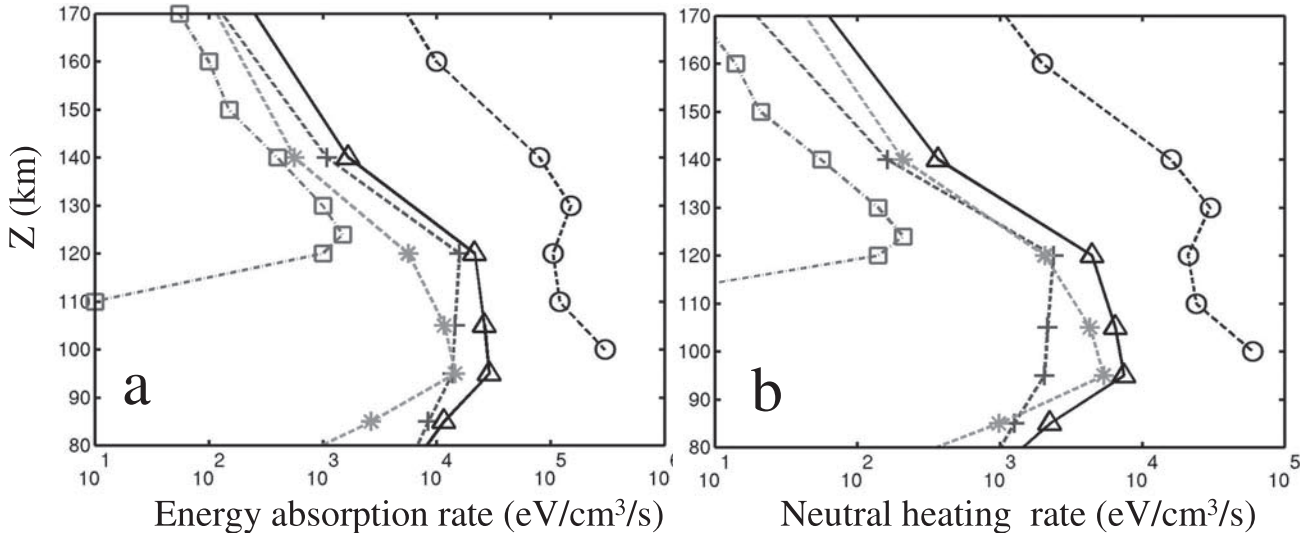

Figure 6. (a) Energy deposition into the atmosphere due to the gradual proton event reported Figure 1. (b) Neutral heating rate due to the same event. Stars show energy deposition due to solar energetic particles (SEP) of He particles. Crosses line shows energy deposition due to SEP H particles. Triangles show total energy deposition due to SEP H and He. Squares show energy deposition due to energetic neutral atoms as calculated by *Kallio and Barabash* [2001]. Circles show energy deposition due to EUV/UV flux [*Fox and Dalgarno*, 1979].

agreement with *Kallio and Barabash* [2001]. However, the amount of backscattering is very different; SRIM gives 10%, whereas *Kallio and Barabash* [2001] found that 58% of the incident H are backscattered. Although the atomic model will underestimate this slightly, the 58% value is too large. The direct neutral heating by elastic collisions decreases with larger impacting energy; at 5 keV an H particle loses only 6.6% of its energy in elastic collisions, whereas at 5 keV, He loses 37% in elastic collisions. In Figure 6b the net neutral heating is obtained by multiplying the energy deposit by 0.2 for the EUV/UV source [*Fox et al.*, 1995], by 0.14 for the ENA energy deposition [*Kallio and Barabash*, 2001], and by 0.12 and 0.3 for the H and He neutral heating efficiency. The H and He heating efficiency are deduced from SRIM calculation and correspond to the average neutral heating efficiency of H particles of energy between 0.5 and 10 keV and for the He particles between 3 and 20 keV. Indeed, the energy deposition is mainly coming from particles with energy in these ranges of energy.

[31] In Figure 6b we compare the solar wind heating rate [*Kallio and Barabash*, 2001] with the heating rate due to the SEP event of Figure 1. The heating rate due to SEP (triangles) is 1 order of magnitude greater than that due to ENA (squares). Figure 6b also shows that the SEP helium heating (stars) is larger than that for H (crosses). The peak heating due to H and He SEPs between 120 and 105 km in altitude corresponds to 4×10^3 eV/cm^3/s, whereas the EUV/UV heating rate is equal to 2×10^4 eV/cm^3/s. This is an increase of $\sim$20% in the heating of the neutral atmosphere just below the homopause. To this neutral heating should also be added the heating due to ionization and excitations. The efficiency of this form of heating of the neutral atmosphere should be close to that determined by *Fox et al.* [1995], as the EUV/UV radiation also ionizes and excites the gas. According to *Kallio and Barabash* [2001], $\sim$26% of the energy of the impacting solar wind proton is deposited into ionization, which then could lead to $\sim$5% of the total energy deposition leading to neutral heating. Therefore a conservative estimate is that SEPs increase the heating rate by $\sim$30%.

[32] In this work we consider an IMF orientation which generates the smallest capture efficiency of solar particles. Indeed *Brecht* [1997b] showed that such efficiency varies from 3 to 30% when the IMF orientation changes from 90° (angle here considered) to 0° for the same solar wind ram pressure. Therefore the neutral heating due to SEP particles could be much larger in some more favorable case of magnetic field orientation than in the case presented in Figure 6b.

3.4. Effect of the Crustal Magnetic Field

[33] We also investigated the local shielding due to the crustal magnetic field [*Acuña et al.*, 2001]. Figure 7a illustrates this magnetic field as interpolated from Mars spacecraft measurements to 200 km from Mars' surface by *Purucker et al.* [2000]. The highest field anomalies are in the Southern Hemisphere and are arbitrarily placed at 0° in longitude in Figure 7a and can have intensities up to 500 nT. Such fields can protect Mars' atmosphere from the impacting ions. In order to investigate the extent of this effect, we use the method of section 2.1 but change the magnetic field model to that of *Purucker et al.* [2000] and neglect the magnetosheath field. Thousands of ions are launched around Mars, covering all geographical latitudes and longitudes. The flux is determined at 200 km above the surface, where the ions that mainly contribute to atmospheric heating (i.e., with energy smaller than few keV/amu) are assumed to be fully neutralized. We follow only the protons and alpha particles since they are primarily responsible for atmospheric heating. The SEP flux at 200 km normalized by its maximum and with respect to latitude and longitude is displayed in Figure 7b. The expected correlation between local shielding and strong crustal magnetic field anomalies is seen. The crustal magnetic field thus protects Mars' atmosphere from impacting particles in some locales. The regions of strongest magnetic anomalies are totally protected from this flux. It is also interesting that a significant maximum of incident flux appears around 0° in longitude and $-50°$ latitude due to the deflection of incident particles from regions at $-40°$ and $-60°$ latitudes, corresponding to the strong crustal magnetic field anomalies. A consequence of the local shielding and deflection can be the creation of strong local winds around the homopause in the regions of crustal magnetic anomalies due to the nonuniform spatial deposition of the SEP energy.

3.5. Flux at the Surface

[34] The model described in the section 3.4 also gives the energy flux reaching the surface. In general, H atoms or protons of energy >83 MeV have enough energy to penetrate Mars'

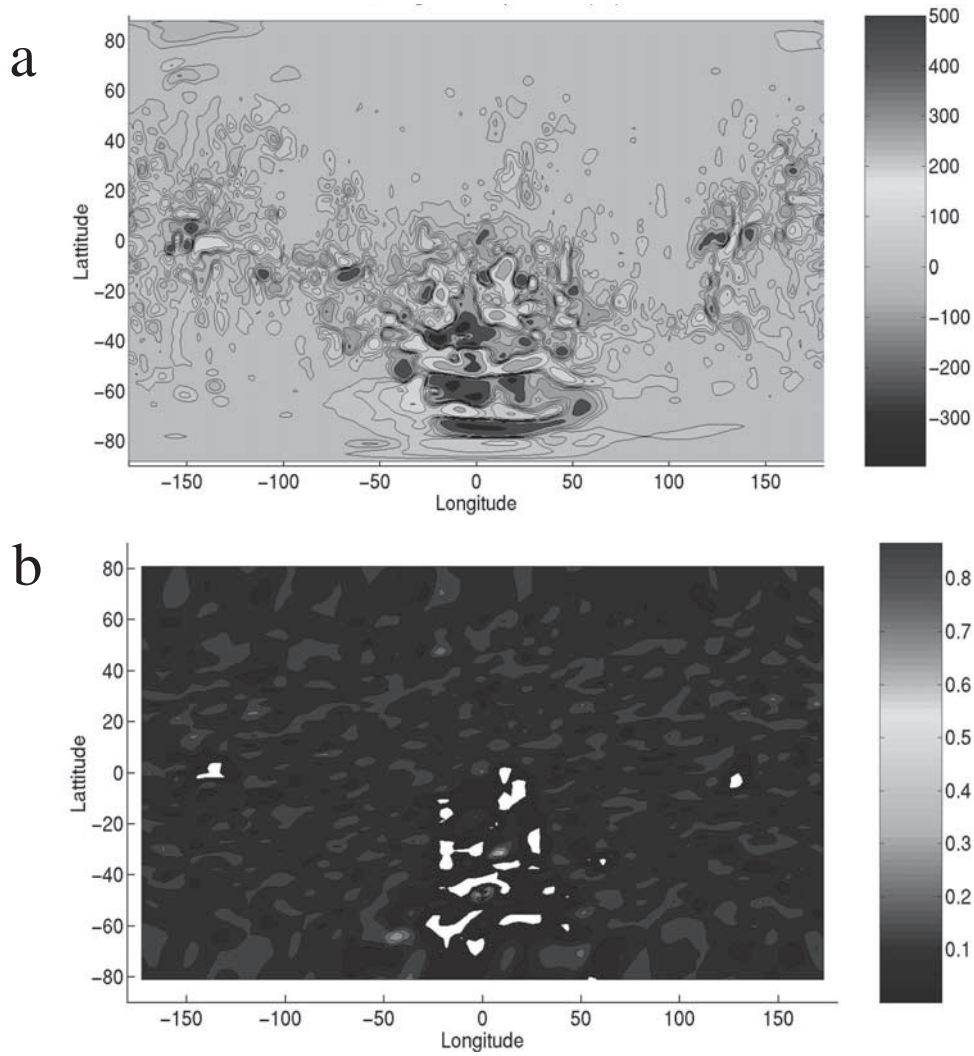

Figure 7. (a) Magnetic crustal field at 200 km from the Martian surface as calculated by *Purucker et al.* [2000]. (b) Distribution of the flux normalized by its maximum (2×10^8 keV/cm^2/s) reaching the exobase and deflected by the crustal magnetic field.

atmosphere. A particle of lower energy will be thermalized by collisions with the atmospheric particles before reaching the surface. The heavier particles C and O are also efficiently stopped by Mars' atmosphere and helium particles need more than 335 MeV to reach the surface. Therefore the flux of protons to the surface is the most important one. Above a few hundred keV an incident particle is essentially not deflected by the magnetic pileup and bow shock and do not charge exchange efficiently with atmospheric neutrals. Therefore the results are not dependent on the model of the magnetosheath and neutralization effect, although the exposure of the dayside and nightside of Mars will depend on the incident SEP's degree of isotropy and shadowing by the planet.

[35] Figure 8 shows the energy flux reaching the surface associated with the gradual proton event provided in Figure 1. Unlike the heating the energy flux to the surface (integrated over all the energies up to 160 MeV) does not vary significantly due to the crustal magnetic field anomalies because H particles with energy larger or equal than 83 MeV are not significantly affected by the crustal magnetic field. Therefore the whole surface of Mars is almost homogeneously exposed to the flux shown in Figure 8. As soon as a flux of SEPs with energy around 100 MeV reaches Mars, a flux of protons with energy $\sim$5–30 MeV should be expected at the surface (which are particles of initial energy >83 MeV losing $\sim$95% of this energy). Protons of energy around 30 MeV are dangerous for human exploration of Mars [*Feynman and Gabriel*, 2000].

4. Conclusion

[36] The observation of the encounter of a solar energetic particle (SEP) event, such as a gradual proton event, with Mars can indicate the effect of the space environment on the Martian atmosphere. In this paper we estimate the size of the effects expected by such an interaction. A simple model of the draped magnetic field lines due to the encounter of the slow solar wind with Mars is used to describe the bow shock and magnetic pileup at Mars [*Luhmann et al.*, 2002]. Test particles representative of the SEP event reported by *Reames et al.* [1997a] are followed until they either reach the Martian exobase or leave the vicinity of Mars. In this paper we show how SEPs penetrate the bow shock and magnetosheath barrier. We also investigate the effect of the crustal magnetic field [*Acuña et al.*, 2001; *Purucker et al.*, 2000]. We calculated atmospheric sputtering, heating rates, and the irradiation of the surface by SEPs.

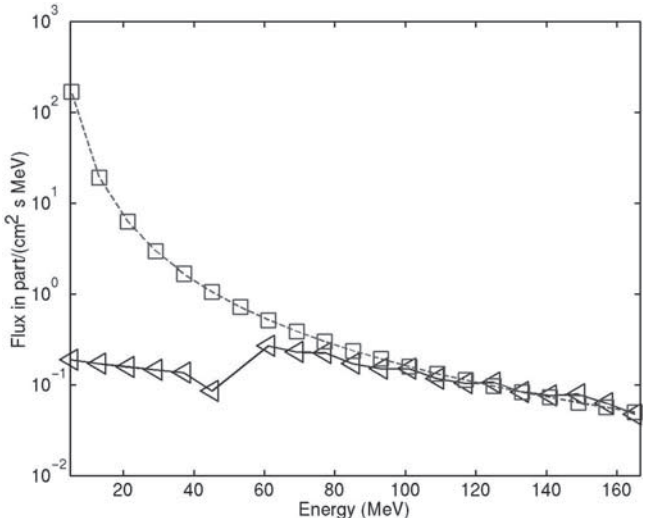

Figure 8. Energy distribution of the solar energetic hydrogen flux reaching the surface. Squares show initial GPE flux of H^+ before Mars' bow shock. Triangles show final flux of H reaching Mars' surface.

[37] According to these calculations, an orbiting instrument measuring particle fluxes in the magnetotail could observe an increase in the flux of escaping neutrals (in particular, an increase of the flux of neutral CO molecules). An increase of the ion flux (not estimated in this paper) is also expected due to the energetic electrons associated with the CME magnetic cloud "sheath", the region of increased solar wind density due to compression by the ejecta moving through it. At the homopause (around 120 km) an increase in the energy deposition rate of the order of the solar EUV/IR heating rate will be seen and possibly associated with winds in the upper atmosphere regions close to the strongest crustal magnetic field anomalies [*Purucker et al*., 2000]. A surface instrument on the Martian dayside would measure H atoms fluxes of 0.1 particles/cm^2/s with energies from 5 up to 160 MeV plus associated secondary particles. This will last tens of hours in the case of a SEP event like the one reported by *Reames et al.* [1997a]. An imaging UV spectrometer should also observe significant increases of the Lyman α emission on the Martian dayside.

[38] In this paper we have neglected the effects due to the arrival of the shock and magnetic cloud associated with a gradual proton event on the magnetic field draping around Mars and also the reconnection of the interplanetary magnetic field with the crustal field, which could have important local effects [*Brain et al.*, 2001; *Luhmann et al.*, 2002]. The later arrival of the interplanetary shock and magnetic cloud [*Burlaga*, 1991], which has a much more intense interplanetary magnetic field, can also produce observable effects at Mars. At the moment of the encounter the magnetosheath field pileup can increase due to the compression from the high solar wind dynamic pressure behind the shock, or the magnetosheath can expand due to the higher upstream Alfvén Mach number. The way that the shielding of Mars' atmosphere changes in such cases is therefore not straightforward and will need accurate observational and modeling studies.

[39] We have also neglected in this paper any kind of feedback processes. The increase of the density in the upper atmosphere due to the impact of the incident particles into Mars' atmosphere [*Leblanc and Johnson*, 2001] is not included. Moreover, the heating near the homopause that has been calculated could change the higher altitude pressure equilibrium with the solar wind ram pressure outside of magnetically dominated regions of the solar wind interaction boundary. The increase of the pickup ion population generated by charge exchange and electron impact would modify the magnetic field draping around Mars, though this may not be important for the large gyroradius particles we consider here. We have also not considered details of the atmospheric dynamical or chemical response.

[40] A self-consistent model is needed to treat accurately the mass loading and the magnetic field draping due to the interplanetary shock, the magnetic cloud, and the change in the upper atmosphere pressure associated with a SEP event. Here we have given a first order approximation of the space weather effects on Mars from such an encounter only to illustrate the potential importance, breadth, and interest of such effects for future exploration and study.

[41] **Acknowledgments.** We would like to thank M. Purucker, D. Ravat, H. Frey, C. Voorhies, T. Sabaka, and M. Acuña for providing the model of crustal magnetic field at Mars, which was shown in Figure 7a. The work at the University of Virginia was supported by the NSF Astronomy Division and by NASA's Planetary Atmospheres Program.

[42] Michel Blanc thanks two anonymous reviewers for their assistance in evaluating this paper.

References

Acuña, M. H., et al., Magnetic field of Mars: Summary of results from the aerobreaking and mapping orbits, *J. Geophys. Res.*, *106*, 23,403–23,417, 2001.

Baring, M. G., K. W. Ogilvie, D. C. Ellison, and R. J. Forsyth, Acceleration of solar wind ions by nearby interplanetary shocks: Comparison of Monte Carlo simulation with Ulysses observations, *Astrophys. J.*, *476*, 889–902, 1997.

Bauske, R., A. F. Nagy, T. I. Gombosi, D. L. De Zeeuw, K. G. Powell, and J. G. Luhmann, A three-dimensional MHD study of the solar wind mass loading processes at Venus: Effects of photoionization, electron impact ionization, and charge exchange, *J. Geophys. Res.*, *103*, 23,625–23,638, 1998.

Bird, G. A., *Molecular Gas Dynamics and the Direct Simulation of Gas Flows,* Clarendon, Oxford, England,1994.

Bougher, S. W., and R. G. Roble, Comparative terrestrial planet thermosphere, 1, Solar cycle variation of global mean temperature, *J. Geophys. Res.*, *96*, 11,045–11,055, 1991.

Brain, D. A., F. Bagenal, D. H. Acuña, J. E. P. Connerney, D. H. Crider, D. L. Mitchell, and J. G. Luhmann, Reconnection of Martian crustal magnetic fields to solar wind, *Geophys. Res. Abstr.*, *3*, 7378, 2001.

Brecht, S. H., Hybrid simulations of the magnetic topology of Mars, *J. Geophys. Res.*, *102*, 4743–4750, 1997a.

Brecht, S. H., Solar wind proton deposition into the Martian atmosphere, *J. Geophys. Res.*, *102*, 11,287–11,294, 1997b.

Burlaga, L. F. E., Magnetic clouds, in *Physics of the Inner Heliosphere II*, edited by R. Schwenn and E. Marsch, Springer-Verlag, New York, 1991.

Eckstein, W., *Computer Simulation of Ion-Solid Interactions*, Springer-Verlag, New York, 1991.

Ellison, D. C., and R. Ramaty, Shock acceleration of electrons and ions in solar flares, *Astrophys. J.*, *298*, 400–408, 1985.

Feynman, J., and S. B. Gabriel, On space weather consequences and predictions, *J. Geophys. Res.*, *105*, 10,534–10,536, 2000.

Feynman, J., G. Spitale, J. Wang, and S. Gabriel, Interplanetary proton fluence model: JPL 1991, *J. Geophys. Res.*, *98*, 13,281–13,294, 1993.

Fox, J. L., and A. Dalgarno, Ionization, luminosity, and heating of the upper atmosphere of Mars, *J. Geophys. Res.*, *84*, 7315–7333, 1979.

Fox, J. L., P. Zhou, and S. W. Bougher, The Martian thermosphere/ionosphere at high and low solar activities, *Adv. Space Res.*, *17*, 203–208, 1995.

Gosling, J. T., and D. J. McComas, Field line draping about fast coronal mass ejecta: A source of strong out-of-the-ecliptic interplanetary magnetic fields, *Geophys. Res. Lett.*, *14*, 355–358, 1987.

Gosling, J. T., J. R. Asbridge, S. J. Bame, W. C. Feldman, R. D. Zwickl, G. Paschmann, N. Skopke, and R. J. Hynds, Interplanetary ions during an energetic storm particle event: The distribution function from solar wind thermal energies to 1.6 MeV, *J. Geophys. Res.*, *86*, 547–554, 1981.

Johnson, R. E., *Energetic Charged-Particle Interactions With Atmospheres and Surfaces*, Springer-Verlag, New York, 1990.

Johnson, R. E., and M. Liu, The loss of atmosphere from Mars, *Science*, *274*, 1932, 1996.

Johnson, R. E., and M. Liu, Sputtering of the atmosphere of Mars, 1, Collisional dissociation of CO_2, *J. Geophys. Res.*, *103*, 3639–3647, 1998.

Johnson, R. E., and J. G. Luhmann, Sputter contribution to the atmospheric corona on Mars, *J. Geophys. Res.*, *103*, 3649–3653, 1998.

Johnson, R. E., D. Schnellenberger, and M. C. Wong, The sputtering of an oxygen thermosphere by energetic O^+, *J. Geophys. Res.*, *105*, 1659–1670, 2000.

Jones, F. C., and D. C. Ellison, The plasma physics of shock acceleration, *Space Sci. Rev.*, *58*, 259–346, 1991.

Kallio, E., and S. Barabash, Atmospheric effects of precipitating energetic hydrogen atoms on the Martian atmosphere, *J. Geophys. Res.*, *106*, 165–178, 2001.

Kallio, E., and H. Koskinen, A test particle simulation of the motion of oxygen ions and solar wind protons near Mars, *J. Geophys. Res.*, *104*, 557–580, 1999.

Kallio, E., and J. G. Luhmann, Charge exchange near Mars: The solar wind absorption and energetic neutral atom production, *J. Geophys. Res.*, *102*, 22,183–22,198, 1997.

Kallio, E., J. G. Luhmann, and J. G. Lyon, Magnetic field near Venus: A comparison between Pioneer Venus Orbiter magnetic field observations and a MHD simulation, *J. Geophys. Res.*, *103*, 4723–4737, 1998.

Kass, D. M., and Y. L. Yung, Loss of atmosphere from Mars due to solar-wind induced sputtering, *Science*, *268*, 697–699, 1995.

Kass, D. M., and Y. L. Yung, The loss of atmosphere from Mars: Response, *Science*, *274*, 1932–1933, 1996.

Kim, J., A. F. Nagy, J. L. Fox, and T. E. Cravens, Solar cycle variability of hot oxygen atoms at Mars, *J. Geophys. Res.*, *103*, 29,339–29,342, 1998.

Klein, K.-L., and G. Trottet, The origin of solar energetic particle event: Coronal acceleration versus shock wave acceleration, *Space Sci. Rev.*, *95*, 215–225, 2001.

Leblanc, F., and R. E. Johnson, Sputtering of the Martian atmosphere by solar wind pick-up ions, *Planet. Space Sci.*, *49*, 645–656, 2001.

Leblanc, F., and R. E. Johnson, Role of molecular species in pickup ion sputtering of the Martian atmosphere, *J. Geophys. Res.*, *107*(E2), 10.1029/2000JE001473, 2002.

Lee, M. A., Particle acceleration and transport at CME-driven shocks, *Coronal Mass Ejections*, *Geophys. Monogr. Ser.*, vol. 99, edited by N. Crookeret et al., pp. 227–234, AGU, Washington, D.C., 1997.

Lin, R. P., Energetic solar electrons in the interplanetary medium, *Sol. Phys.*, *100*, 537–561, 1985.

Luhmann, J. G., and J. U. Kozyra, Dayside pickup oxygen in precipitation at Venus and Mars: Spatial distribution, energy deposition, and consequences, *J. Geophys. Res.*, *96*, 5457–5467, 1991.

Luhmann, J. G., M. Tatrallyay, C. T. Russell, and D. Winterhalter, Magnetic field fluctuations in the Venus magnetosheath, *Geophys. Res. Lett.*, *10*, 655–658, 1983.

Luhmann, J. G., R. E. Johnson, and M. H. G. Zhang, Evolutionary impact of sputtering of the Martian atmosphere by O^+ pickup ions, *Geophys. Res. Lett.*, *19*, 2151–2154, 1992.

Luhmann, J. G., M. H. Acuña, M. Purucker, C. T. Russell, and J. G. Lyon, The Martian magnetosheath: How Venus-like?, *Planet. Space Sci.*, in press, 2002.

Mason, G. L., et al., Particle acceleration and sources in the November 1997 solar energetic particle event, *Geophys. Res. Let.*, *26*, 141–144, 1999.

McKenna-Lawlor, S., V. V. Afonin, E. Kirsch, K. Schwingenschuh, J. A. Slavin, and J. G. Trotignon, An overview of energetic particles (from 55 keV to >30 MeV) recorded in the close Martian environment and their energization in local and external processes, *Planet. Space Sci.*, *46*, 83–102, 1998.

Oetlicker, M., B. Klecker, D. Hovestadt, G. M. Mason, J. E. Mazur, R. A. Leske, R. A. Mewaldt, J. B. Blake, and M. D. Looper, The ionic charge of solar energetic particles with energies of 0.3-70 MeV per nucleon, *Astrophys. J.*, *477*, 495–501, 1997.

Purucker, M., D. Ravat, H. Frey, C. Voorhies, T. Sabaka, and M. Acuňa, An altitude-normalized magnetic map of Mars and its interpretation, *Geophys. Res. Lett.*, *27*, 2449–2452, 2000.

Reames, D. V., Solar energetic particles: A paradigm shift, *Rev. Geophys.*, *30*, 585–590, 1995.

Reames, D. V., Particle acceleration at the sun and in the heliosphere, *Space Sci. Rev.*, *413*, 413–491, 1999.

Reames, D. V., L. M. Barbier, T. T. von Rosenvinge, G. M. Mason, J. E. Mazur, and J. R. Dwyer, Energy spectra of ions accelerated in impulsive and gradual solar events, *Astrophys. J.*, *483*, 515–522, 1997a.

Reames, D. V., S. W. Kahler, and C. K. Ng, Spatial and temporal invariance in the spectra of energetic particles in gradual solar events, *Astrophys. J.*, *491*, 414–420, 1997b.

Reames, D. V., C. K. Ng, and A. J. Tylka, Heavy ion abundances and spectra and the large gradual solar energetic particles event of 2000 July 14, *Astrophys. J.*, *548*, L233–L236, 2001.

Russell, C. T., T. L. Zhang, and J. G. Luhmann, On the cause of distant bow shock encounters, in *Plasma Environments of the Nonmagnetic Planets*, edited by T. I. Gombosi, Pergamon, New York, 1993.

Van Nes, P., R. Reinhard, T. R. Sanderson, and K.-P. Wenzel, The energy spectrum of 35- to 1600-keV protons associated with interplanetary shocks, *J. Geophys. Res.*, *89*, 2122–2132, 1984.

Von Steiger, R., J. Geiss, G. Gloecker, and A. B. Galvin, Kinetic properties of heavy ions in the solar wind from SWICS/Ulysses, *Space Sci. Rev.*, *72*, 71–XX, 1995.

Von Steiger, R., N. A. Schwadron, L. A. Fisk, J. Geiss, G. Gloecker, S. Hefti, B. Wilken, R. F. Wimmer-Schweingruber, and T. H. Zurbuchen, Composition of quasi-stationary solar wind flows from Ulysses/Solar wind ion composition spectrometer, *J. Geophys. Res.*, *105*, 27,217–27,238, 2000.

Zhang, M. H. G., J. G. Luhmann, A. F. Nagy, J. R. Spreiter, and S. Stahara, Oxygen ionization rates at Mars and Venus: Relative contributions of impact ionization and charge exchange, *J. Geophys. Res.*, *98*, 3311–3318, 1993.

Ziegler, J. F., J. P. Biersack, and V. Littmark, The Stopping and Ranges of Ions in Solids, Pergamon, New York, 1985.

E. Chassefiere and F. Leblanc, Service d'Aéronomie du CNRS, Réduit de Verrières-Le-Buisson, BP 3, F-91371 Verrières-Le-Buisson, France. (eric.chassefiere@aero.jussieu.fr; francois.leblanc@aerov.jussieu.fr)

R. E. Johnson, Materials Science and Engineering Department, University of Virginia, Thornton Hall B103, Charlottesville, VA 22903, USA. (rej@virginia.edu)

J. G. Luhmann, Space Science Laboratory, University of California, Berkeley, Centennial Drive at Grizzly Peak Blvd., Berkeley, CA 94720-7450, USA. (jgluhman@ssl.berkeley.edu)